
The Geometry of Self-Verification in a Task-Specific Reasoning Model

Andrew Lee[§], Lihao Sun[¶], Chris Wendler^{¶†}, Fernanda Viégas^{§,¶*}, Martin Wattenberg^{§,¶*}

[§]Harvard University, [¶]University of Chicago, [†]Northeastern University, [¶]Google DeepMind
andrewlee@g.harvard.edu

Abstract

How do reasoning models verify their own answers? We study this question by training a model using DeepSeek R1’s recipe on the Countdown task. We leverage the fact that preference tuning leads to mode collapse, resulting in a model that always produces highly structured and easily parse-able chain-of-thought sequences. With this setup, we do a top-down and bottom-up analysis to reverse-engineer how the model verifies its outputs. Our top-down analysis reveals Gated Linear Unit (GLU) weights encoding verification-related tokens, such as “success” or “incorrect”, which activate according to the correctness of the model’s reasoning steps. Our bottom-up analysis reveals that “previous-token heads” are mainly responsible for model verification. Our analyses meet in the middle: drawing inspiration from inter-layer communication channels, we use the identified GLU vectors to localize as few as three attention heads that can disable model verification, pointing to a necessary component of a potentially larger verification circuit.

1 Introduction

Recent language models like OpenAI’s o-series [27] and DeepSeek R1 [11] demonstrate impressive reasoning capabilities. Such models are trained with reinforcement learning (RL) in which they are rewarded when their final outputs are correct.

Behaviorally, these models generate long chain-of-thought (CoT) [38] reasoning traces. There is an open question on whether monitoring their CoT is worthwhile, given a growing line of work suggesting that their CoTs do not faithfully reflect the model’s inner computations [2, 14, 36]. Can we monitor their hidden states instead? We take a step towards investigating this question, by studying a model’s inner mechanism for a crucial reasoning step, i.e., self-verification.

General reasoning entails a broad range of tasks, requiring a diverse set of skills. In order to conduct a systematic study, we train and analyze a task-specific reasoning model using the same recipes from DeepSeek R1. We limit the scope of our study to a specific task that requires search – a core reasoning skill broadly applicable for many reasoning tasks. We also select a task in which we can expect the verification mechanism ahead of time, making our analyses easier. Namely, we study Countdown [9, 10, 31, 39], in which a set of numbers (operands) and a target number is given, and the model must find the right arithmetic combination using the operands to reach the target number. Because the target number is specified in the context, we can expect attention heads to play a role in verification and shed light onto other relevant weights and subspaces pertaining to self-verification.

Studying a task-specific model has a second non-obvious benefit: training language models with RL (i.e., with preference signals) can lead to mode collapse towards majority preferences, significantly

*Work done entirely at Harvard.

This project was done as part of ARBOR. For more information, see <https://arborproject.github.io/>

reducing the diversity of their outputs [13, 21, 29, 34]. Luckily, in the context of model interpretability, this means that our task-specific model converges to always generating well-structured CoT sequences, allowing us to easily and systematically parse its reasoning trace (e.g., see Table 1).

Given our setup, we conduct “top-down” and “bottom-up” analyses to reverse-engineer how the model verifies its own predictions. Our two analyses meet in the middle, revealing key subspaces relevant for model verification.

Going top-down, we leverage linear probes to find Gated Linear Unit (GLU) vectors in late layers that each activate given correct or incorrect attempts in the model’s CoT. Not only do these vectors often encode tokens relevant for verification, but the vectors for correct and incorrect cases also seem to correlate with English or Chinese tokens, like “success” or “不完” (“failed”). Furthermore, the antipodal directions of these vectors also encode the antonyms of correct or incorrect tokens.

Going bottom-up, given the nature of our task, we hypothesize and verify that attention heads play a significant role. We find “previous-token heads” – attention heads that attend to previous occurrences of the current token – that attend to the provided solution in the context. Previous-token heads have been studied before, for instance in the context of induction heads [26]. Through causal analyses, we find that disabling previous-token heads disables model verification.

Our two analyses meet in the middle: we find that disabling previous-token heads also deactivates our GLU vectors. Inspired by inter-layer communication channels [7, 19], we look for previous-token heads that most align with the “receptive-field” of our GLU vectors, allowing us to localize as few as three attention heads that reliably disables model verification. Thus our work finds necessary components for a potentially larger verification circuit.

Obviously, most reasoning tasks do not provide an easily verifiable solution in the context. However, we expect many of the same components and subspaces to be used in other reasoning tasks [16]. By illustrating a thorough mechanism of verification in our simplified setup, we take a step towards the possibility of monitoring and interpreting a model’s inner computations in its hidden states.

2 Notations, Key Terminologies

We first establish some terminologies that we will use, along with notations. The Transformer’s forward pass first embeds each input token using weights $\mathbf{W}_E \in \mathbb{R}^{d \times V}$. The embeddings go through L Transformer blocks, resulting in hidden states $\mathbf{x}^\ell \in \mathbb{R}^d, \ell \in [L - 1]$. The last layer, \mathbf{x}^{L-1} , is “unembedded”, or projected back to the model’s token embedding space using \mathbf{W}_E , and the nearest neighboring token embedding of $\mathbf{W}_E^\top \mathbf{x}^{L-1}$ is selected as the next token to be predicted. Each Transformer block consists of attention heads and MLP blocks, with recent models replacing MLPs with Gated Linear Units (GLUs) [33].

Attention. Each attention head consists of key (W_K), query (W_Q), value (W_V), and output (W_O) weights. an attention pattern A is computed using key and query weights:

$$A = \text{softmax}(\mathbf{x}_i^\top W_Q^\top W_K \mathbf{x}_i) \quad (1)$$

where $W_Q^\top W_K$ is sometimes referred to as a “QK circuit”. A is used to scale the “OV circuit” ($W_O W_V$) to produce an output for each head:

$$h(\mathbf{x}) = (A \otimes W_O W_V) \cdot \mathbf{x} \quad (2)$$

Gated Linear Units and GLU_{Out} Vectors. Given a Gated Linear Unit (GLU) block:

$$\text{GLU}(\mathbf{x}) = (\sigma(W_{gate}\mathbf{x}) \odot W_{up}\mathbf{x}) W_{out} \quad (3)$$

$$(4)$$

where $W_{gate}, W_{up}, W_{out} \in \mathbb{R}^{d_{glu} \times d}$, we decompose it as following:

$$M = \sigma(W_{gate}\mathbf{x}) \odot W_{up}\mathbf{x}, M \in \mathbb{R}^{d_{glu}}, \quad (5)$$

$$\text{GLU}(\mathbf{x}) = M^\top W_{out} = \sum_j^{d_{glu}} m_j \mathbf{v}_j \quad (6)$$

where m_j is the j -th entry in M and \mathbf{v}_j is the j -th row of W_{out} .

Importantly, the output of each GLU block can be thought of as the weighted sum of \mathbf{v} (the rows of W_{out}), where the weights are determined by activations M . **We refer to elements of M as GLU neurons and vectors \mathbf{v} as GLU_{out} vectors.** For more details, we refer readers to [7].

3 Training Task-Specific Reasoning Models

We train our model using DeepSeek R1-Zero’s setup.² We use Qwen2.5-3B as our base model, which consists of 36 layers and 16 attention heads per layer.

Our task, CountDown, is a simple testbed frequently used to study recent reasoning models [9, 10, 31, 39] – given a set of 3 or 4 operands (e.g., 19, 36, 55, 7) and target number (e.g., 65), the task is to find the right arithmetic combination of the operands to reach the target number (i.e., $55 + 36 - 7 - 19$).

The model is given two rewards: accuracy reward for reaching the correct final answer, and a format reward when it generates its CoT tokens in between “<think>” and “</think>” tokens. For details on how R1-Zero is trained, see [11].

One advantage of studying a specific task is in that preference training leads to mode collapse [13, 21, 29, 34], resulting in a reduction in generation diversity. In our context, this is desirable, as the model converges to generating a highly structured CoT sequence. See Table 1.

This allows us to easily parse the model’s CoT. Namely, the model enumerates through many attempts, while always marking each attempt as either “(this works)” or “(not {ans})”. Thus, we can study the model’s hidden states at specific timesteps, such as right before it produces either “not” or “this”, which we refer to as $t_{invalid}$ and t_{valid} . We refer to the hidden states at these timesteps as $\mathbf{x}_{Invalid}$ and \mathbf{x}_{Valid} . We refer to the timestep in the prompt at which the target number is specified as t_{ans} .

A conversation between User and Assistant. The user asks a question, and the Assistant solves it. The assistant first thinks about the reasoning process and then provides the user with the answer.

User: Using the numbers [20, 14, 40], create an equation that equals 28. You can use basic arithmetic operations (+, -, *, /) and each number can only be used once. Show your work in <think> </think> tags. And return the final answer in <answer> </answer> tags, for example <answer> (1 + 2) / 3 </answer>.

Assistant: Let me solve this step by step. <think> We have the numbers 20, 14, and 40. We need to use these numbers to make an equation that equals 28 using basic arithmetic operations. Let’s try different combinations:
- 40 - 14 - 20 = 10 - 20 = -10 (not 28)
- 40 - 14 + 20 = 26 + 20 = 46 (not 28)
- 40 + 14 - 20 = 54 - 20 = 34 (not 28)
- 40 + 14 + 20 = 54 + 20 = 74 (not 28)
- 40 * 14 / 20 = 560 / 20 = 28 (**this works**)
So, the equation that equals 28 is 40 * 14 / 20. </think> <answer> (40 * 14) / 20 </answer>

Table 1: **CountDown Task.** The model must use the operands to reach the specified target number using arithmetic operations. We leverage the fact that preference tuning leads to mode collapse, resulting in consistently generating nicely structured CoT tokens that we can easily parse.

4 Components for Verification in CountDown

Here we present a series of analyses to identify weights and subspaces relevant for verification. We do a “top-down” analysis to find relevant GLU vectors in late layers, and a “bottom-up” analysis to find relevant attention heads in early layers. Our analyses meet in the middle, to identify relevant subspaces for verification. We verify the role of such weights and subspaces via causal experiments.

²We use TinyZero: <https://github.com/Jiayi-Pan/TinyZero/tree/main>



Figure 1: **Averaged LogitLens from 300 samples.** We see tokens related to verification (“success”, “incorrect”) in the last few layers. (A), (B) show the top tokens when a correct / incorrect solution is reached. (C), (D) shows results from intervening on either GLU weights or attention heads, given a correct solution. For (C), while the model is less certain (P(“this”) versus P(“not”) becomes 0.51 vs. 0.49 in last layer), we still see tokens such as “success” showing up. For (D), we no longer see any tokens related to “success” show up, and the model is certain that it has not found a solution.

4.1 Top-Down: Finding Verification-Related GLU Vectors

LogitLens. We start our analysis by applying LogitLens [23] to compare the hidden states of $\mathbf{x}_{\text{Valid}}$ and $\mathbf{x}_{\text{Invalid}}$ on a sample size of 300. We apply the unembedding layer at all intermediate layers \mathbf{x}^ℓ and inspect the resulting nearest neighboring tokens across 300 samples.

Figure 1(A, B) shows our results in the late layers. Interestingly, we see tokens such as “SUCCESS”, “yes”, “OK”, “bingo” show up for $\mathbf{x}_{\text{Valid}}$, and “不符合” (“Does not conform”), “不行” (“Not okay”), “不合” (“Incompatible”) for $\mathbf{x}_{\text{Invalid}}$. Interestingly, we often observe English tokens for $\mathbf{x}_{\text{Valid}}$ and Chinese tokens for $\mathbf{x}_{\text{Invalid}}$. What drives these tokens to appear?

Probing. To answer this question, we train linear probes $W^\ell \in \mathbb{R}^{2 \times d}$ at every layer ℓ from timesteps right before “this” or “not” is predicted (i.e., $t_{\text{valid}} - 1, t_{\text{invalid}} - 1$). These timesteps correspond to when an attempt for a solution has just been made, and an open parenthesis tokens “(” is being predicted as the next token, not when “this” or “not” is being predicted.

Our goal is to learn a linear mapping from the hidden states at these timesteps, \mathbf{x}^ℓ , to a binary label of whether the model has found the solution. Namely, our training data is $\mathcal{D} = \{(\mathbf{x}_{y^i}^\ell, y^i)\}_{i=0}^{N-1}$, where $y^i \in \{0 \text{ (“not”)}, 1 \text{ (“this”)}\}$ and $N = 327,680$. We solve for W^ℓ to fit $y = \text{softmax}(W^\ell \mathbf{x}^\ell)$ using gradient descent (hyperparameters in Appendix A).

Validation accuracy ($N = 512$) per layer is provided in the Appendix (Figure 4), with accuracy usually staying above 90% after the first few layers. High accuracy suggests that our probing vectors

Vector	Nearest Neighbors
$W[0]$ $W[1]$	不完 (unfinished), 不了 (unable), 不 (not), 不在 (absent), 不该 (should not) Exactly, >(, =yes, =YES, =:, ==#, quis, esac, #####
(26, 744) (26, 6619) (27, 9766) (27, 4971)	未能 (failed), 不够 (not enough), nicht (not), 不像 (not like), 达不到 (can't reach) 缺乏 (lack), 缺少 (lack), 不方便 (inconvenient), lacks, 难以 (difficult), 未能 (failed) 是不可能 (impossible), neither, 看不到 (can't see), 不存在 (doesn't exist) inefficient, 没能 (failed), 不方便 (inconvenient), Danger, disadvantage, 不利于
(29, 6676) (27, 10388) (30, 8233)	yes, Yes, Bindable, exactly, Yes, "Yes, yes, Yep, Exactly, included mirac, 乐观 (optimism), 安然 (safely), Relief, 幸 (fortunate), .isSuccess correctly, 正确 (correct), 恰当 (appropriate), accurately, 符合 (conform)
$-1 \times (26, 744)$ $-1 \times (26, 6619)$ $-1 \times (27, 9766)$ $-1 \times (27, 4971)$	慎 (careful), 足 (sufficient), 同等 (equal), tend, ONDON, 足以 (enough) 不仅能 (not only can), 不错的 (good), 具有良好 (have good), 总算 (finally) might, maybe, may, 有时候 (sometimes), 部分地区 (some areas), .some successfully, successful, 顺利 (smooth), 成功 (successful), 删除成功
$-1 \times (29, 6676)$ $-1 \times (27, 10388)$ $-1 \times (30, 8233)$	都不 (neither), 不太 (not quite), neither, 不予 (not given), 没见过 (never seen) 失败 (failure), failure, 不良 (bad), 不利 (unfavorable), 糟糕 (bad), 失误 (mistake) wrong, 不良 (bad), incorrect, wrong, invalid, bad, inappropriate, invalid

Table 2: **GLU_{Out} vectors relevant to verification, and their nearest neighbors.** $W[0], W[1]$ indicate our probe model. “(x, y)” indicates the GLU_{Out} vector at layer x, index y. “ $-1 \times (x, y)$ ” (marked in red) indicates the antipodes of the GLU_{Out} vector at layer x, index y. Interestingly, we observe a correlation between valid/invalid vectors and English and Chinese.

$W[0], W[1]$ identify a direction in the model’s activation space that linearly separates points of $\mathbf{x}_{\text{Valid}}$ and points of $\mathbf{x}_{\text{Invalid}}$ (i.e., linearly separable subspaces).

Such vectors can steer the model. Simply adding $W[0]$ or $W[1]$ into hidden states can push \mathbf{x} towards $\mathbf{x}_{\text{Valid}}$ or $\mathbf{x}_{\text{Invalid}}$, and change the model’s output to indicate that it has (or has not) found a solution, even when it has not (or has). We provide qualitative examples of steering results in Appendix C.

GLU_{Valid}, GLU_{Invalid} Vectors. Our probe W tells us that mid-layer activations can be linearly separated to identify solved cases ($\mathbf{x}_{\text{Valid}}$) from unsolved cases ($\mathbf{x}_{\text{Invalid}}$), but also serves a secondary purpose. Namely, we can use W to identify GLU_{Out} vectors of interest [15].

Per layer, we simply select the top k ($= 50$) GLU_{Out} vectors per layer by how similar they are to $W^\ell[0]$ or $W^\ell[1]$ using cosine similarity scores (Qwen2.5-3B has 11,008 GLU_{Out} vectors per layer). One can consider these top- k GLU_{Out} vectors as weights that contribute the most towards the $W^\ell[0]$ (no solution) or $W^\ell[1]$ (found solution) directions. We refer to GLU_{Out} vectors most similar to $W[0]$ and $W[1]$ as GLU_{Invalid} and GLU_{Valid} vectors. This results in $k \times L \times 2$ GLU_{Out} vectors (0.9% of the model’s GLU_{Out} vectors: $50 \times 36 \times 2 = 3,600$ out of 396,288).

Unembedding GLU_{Valid/Invalid} vectors reveal which tokens get promoted when they are activated. Table 2 shows their nearest neighbors in the model’s token embedding space. We observe that most interpretable GLU_{Out} neurons occur in the second half of layers. Interestingly, we again note that there seems to be a correlation between GLU_{Valid/Invalid} and English versus Chinese tokens, hinting at the underlying geometry of $\mathbf{x}_{\text{Valid/Invalid}}$ and the model’s embedding space.

While the GLU weights encode information that seem relevant for verification, what role do they play? This can partially be answered by applying LogitLens again on 300 samples, but now by “turning off” the GLU_{Valid} vectors ($< 1\%$ of total GLU vectors) by scaling them to zero. Figure 1(C) shows our results: while the probability of verification-related tokens slightly drop (e.g., $P(\text{“SUCCESS”})$ drops from 0.28 to 0.11 in layer 30), the end behavior remains the same (i.e., “this” is still the top-1 token, though $P(\text{“this”})$ drops from 0.98 to 0.51). This tells us that GLUs do not provide a full explanation for verification. We demonstrate a more thorough causal analysis later in the text (Section 4.4).

4.2 Bottom-Up: Previous-Token Attention Heads for Verification (\mathbf{A}_{Prev})

We next inspect the role of attention heads for verification. One motivation for choosing CountDown as our task is that the task specifies the target number in the context. Thus we can posit that a Transformer could verify its CoT tokens by comparing them against the target number (at timestep t_{ans}). Such a hypothesis provides an entry way for our bottom-up analysis. Thus we test our hypothesis by inspecting the attention patterns whenever the model’s CoT produces the correct answer. We filter for attention heads that spend at least 10% of its attention on t_{ans} , and refer to these as previous-token heads (notated \mathbf{A}_{Prev}). Previous-token heads are not new: they were first discussed in the context of induction heads [26]. We identify 25 previous-token heads (out of a total of 576 heads). Interestingly, we find that most previous-token heads occur roughly in the first half layers (except for one at layer 31, all are at or before layer 22). In Section 4.4 we demonstrate via causal interventions that disabling previous-token heads can disable model verification. But first, what is the relationship between $\text{GLU}_{\text{Valid/Invalid}}$ vectors and \mathbf{A}_{Prev} heads? Below we adapt inter-layer component channels to understand their relationship.

4.3 Putting $\text{GLU}_{\text{Valid}}$ and \mathbf{A}_{Prev} Together: Identifying Verification Subspaces (Polytopes)

We identify subspaces for self-verification by studying the relationship between $\text{GLU}_{\text{Valid}}$ vectors and \mathbf{A}_{Prev} attention heads. As a reminder, we observe that previous-token heads usually occur in the first half layers (1 to 22), while $\text{GLU}_{\text{Valid}}$ vectors usually occur in the later half (18 to 36). We hypothesize and empirically verify that \mathbf{A}_{Prev} activates $\text{GLU}_{\text{Valid}}$ vectors.

First, we borrow from neuroscience to define *receptive fields* [25]. Consider a single neuron k , which computes an activation function $f^k : \mathbb{R}^d \rightarrow \mathbb{R}$. A receptive field of neuron k is defined as

$$S_k = \{\mathbf{x} \in \mathbb{R}^d \mid f^k(x) > 0\} \quad (7)$$

In simpler terms, S_k is the subspace that triggers a neuron active. In the context of GLUs, this means

$$S_k = \{\mathbf{x} \in \mathbb{R}^d \mid \sigma(W_{gate}^k \mathbf{x}) \odot W_{up}^k \mathbf{x} > 0\} \quad (8)$$

Now consider a set of neurons, K , and the intersection of all of their receptive fields: $\mathbf{S}_K = \bigcap_i^{|K|} S_i$.

\mathbf{S}_K can be considered a polytope in the model’s activation space parameterized by $\{W_{gate}^i, W_{up}^i\}_{i=1}^{|K|}$. Here we demonstrate that the receptive fields of $\text{GLU}_{\text{Valid}}$ yield polytopes for self-verification.

Namely, we identify a small subset of as few as three previous-token heads that can disable self-verification. To do so, we check how strongly the weights of each previous-token head (as opposed to hidden states) activate $\text{GLU}_{\text{Valid}}$ neurons. The output of each head is its OV-circuit (i.e., $W_O W_V$), scaled according to some attention distribution. Meanwhile, the strength of each $\text{GLU}_{\text{Valid}}$ activation is determined by its gating weights W_{gate} and up-projection weights W_{up} .

We score each previous-token head based on how much they activate $\text{GLU}_{\text{Valid}}$ vectors on average:

$$score(A, \widehat{\text{GLU}}_{\text{Valid}}) = \frac{1}{N} \sum_i^N (\sigma(W_{gate}^i W_O W_V) \cdot W_{up}^i W_O W_V) \quad (9)$$

where $\widehat{\text{GLU}}_{\text{Valid}} = \{W_{gate}^i, W_{up}^i\}_{i=0}^{N-1}$, $N = |\widehat{\text{GLU}}_{\text{Valid}}|$, $W_O W_V$ is the OV circuit of attention head A , and $W_{gate}^i, W_{up}^i, W_O W_V \in \mathbb{R}^d$. Note that this is akin to inter-layer communication channels between model components studied in [7, 19], which scores how strongly two components in different layers communicate with a “composition score”:

$$CS(W_1, W_2) = \frac{\|W_1 W_2\|_F}{\|W_1\|_F * \|W_2\|_F} \quad (10)$$

where W_1 might be an OV component of one head and W_2 the QK component of another at a later layer. Our formulation can be considered a composition score between attention heads and GLUs, using both W_{gate} and W_{up} in place of W_2 with some additional steps in between.

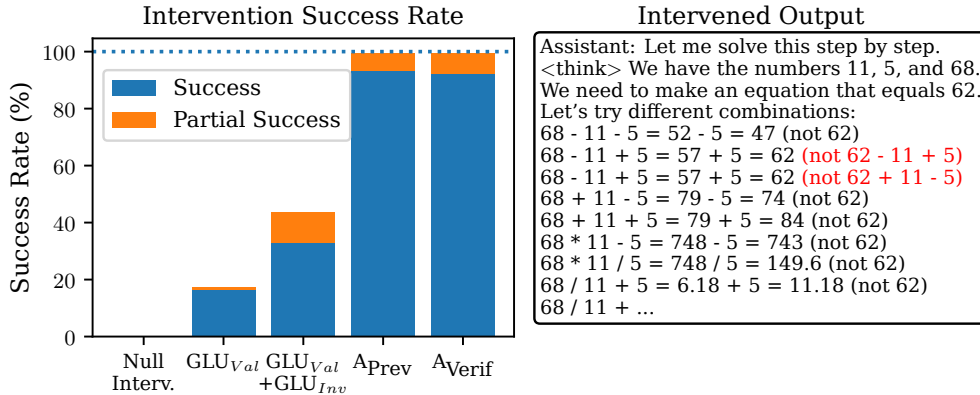


Figure 2: **Intervention Results: Disabling as few as 3 attention heads disables self-verification**, rendering the model to generate tokens indefinitely. A_{Prev} refers to 25 previous-token heads, while A_{Verif} refers to a subset of 3 previous-token heads.

Once we score each previous-token head using Eq. 9, we incrementally ablate one head at a time until we achieve perfect intervention scores (Section 4.4). Using this approach, we identify as few as **three** attention heads that can disable model verification. We notate this subset as A_{Verif} .

To summarize, we claim that the model has subspace(s) (polytope(s)), $S_{\text{GLU}_{\text{valid}}}$, for self-verification. The model’s hidden state enters this subspace when it has verified its solution. In our setting, given the nature of our task, previous-token heads A_{Prev} take the hidden-state into this subspace, while other components may be used for different tasks. This subspace also activates verification-related GLU weights, promoting the likelihood of tokens such as “success” to be predicted.

We add a quick note about localizing attention heads that disable verification. Using different scoring functions, or tweaking hyperparameters (i.e., N), can yield different subsets of heads that can similarly disable model verification. We discuss these results in Appendix D. This suggests that we do not identify a full circuit, but rather critical and necessary components for verification. Also note that our scoring function makes simplifications by ignoring possible interactive effects across heads, and by ignoring transformations (layer norms, GLUs) in between layers. Regardless, our finding remains robust: a small subset of previous-token heads can disable verification.

4.4 Causal Interventions

We study the role of each component above with causal intervention. Our test set consists of 300 samples in which the model originally correctly finds and validates its solutions. For each test case, the model generates 100 tokens. Every time an attempt for a solution is made (i.e., “(this works)” or “(not ({ans}))” is about to be predicted next), we turn off some of the model weights as described below. We measure intervention success rate: the percentage of times the model fails to validate its solution, despite having found the solution within the 100 generated tokens. Interestingly, the model occasionally indicates a correct attempt as invalid (desired intervention result), but continues its generation to say it has found a solution (e.g., given target number 62, the model will output “68 - 11 + 5 = 62 (not 62) So, the answer is 68 - 11 + 5”). We mark these cases as partial successes.

We ablate a few components: (1) **GLU_{valid}**: We zero-out 50 GLU_{valid} vectors per layer from layer 18 to 36 (the second half of the model; 0.45% of all GLU vectors). (2) **GLU_{valid} & GLU_{Invalid}**: We zero-out the top 50 GLU_{valid} and top 50 GLU_{Invalid} vectors per layer (0.9% of all GLU vectors). (3) **A_{Prev}**: We turn off 25 previous-token heads (4.3% of all attention heads) by zeroing-out their W_O weights. (4) **A_{Verif}**: We turn off 3 verification heads identified via Eq. 9: L17H14, L17H11, L17H10.

Results are shown in Figure 2, with an example of an intervened CoT sequence. We can achieve near perfect intervention rates when turning off 25 previous-token heads, or a smaller subset of 3 heads – the model will misclassify correct solutions as invalid without these attention heads.

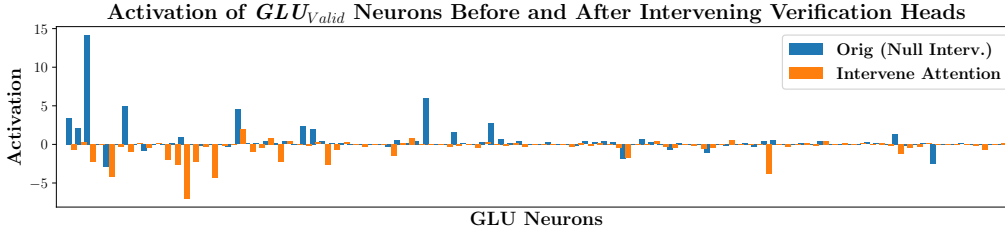


Figure 3: **GLU_{valid} activations before and after turning off 3 attention heads.** Adjacent pairs of blue and orange bars indicate the same GLU_{valid} vector. Turning off our identified attention heads leads to a significant drop in their activations.

These attention heads directly affect the GLU_{valid} vectors. Figure 3 demonstrates the activations of the top GLU_{valid} vectors before and after disabling the subset of 3 previous-token heads. In most cases, we observe a large drop (to near 0, or often even negative values) in GLU_{valid} activations.

Antipodal GLU_{Out} Vectors. While attention heads achieve near perfect interventions, Figure 2 also indicates that disabling both GLU_{valid} and GLU_{Invalid} performs better than disabling just GLU_{valid}. Why should disabling GLU_{Invalid} improve intervening, i.e., make the model fail at verification?

This can be explained by two facts: (1) the geometry of GLU_{valid} and GLU_{Invalid} vectors, and (2) the nonlinear activation used in GLU. Interestingly, we find that the antipodal directions of GLU_{valid} and GLU_{Invalid} also often encode tokens relevant for verification. The last 7 rows of Table 2 marked in red indicate the nearest neighbors of the antipodes of GLU_{valid} and GLU_{Invalid}.

Second, Qwen2.5-3B uses SiLU activations [12]. Thus inactive neurons take on small *negative* values (as opposed to zero, had ReLU been used).

With that said, consider only zeroing out GLU_{valid} neurons: given a correct CoT sequence, GLU_{Invalid} vectors are inactive. However, because of SiLU, the inactive GLU_{Invalid} vectors have negative activations, thus get multiplied by a small *negative* value, flipping directions, and therefore contribute towards the “success direction”. In the case of zeroing out both GLU_{valid} and GLU_{Invalid}, we are further zeroing out the effects of inactive GLU_{Invalid} neurons.

5 Related Work

Recently, there has been many efforts to interpret the inner workings of language models. We broadly categorize such efforts into representation engineering and circuit analyses.

Decoding Interpretable Representations. A popular approach to interpret language models has been to decode and manipulate interpretable representations in the model’s hidden states [41]. Conveniently, many concepts take on *linear* representations [20, 22, 30], in which a single direction encodes human-interpretable concepts. Linear representations allow for easily manipulating the underlying representation to steer the model’s behavior. Examples include refusal [3], sycophancy [32], toxicity [15], sentiment [35], or even representations of the user [5].

In the context of non-reasoning models, researchers have studied “truthful” representations before [4], where steering a model towards a “truthful” direction has led to improvements in tasks such as factual question answering [17]. In a similar vein, researchers have shown that the model’s representations can reveal whether they will make errors (e.g., hallucinations) [28], or when they are unable to recall facts about an entity [8].

Most recently, concurrent work [37, 40] also investigate how models solve reasoning tasks. [40] find that models know when they have reached a solution, while [37] decode directions that mediate behaviors such as handling uncertainty or self-corrections. While our work corroborates these findings, we take a deeper dive into how a reasoning model verifies its own reasoning trace.

Circuit Analysis. A growing line of work decomposes the forward pass of a neural network as “circuits” [24], or computational graphs. This allows researchers to identify key components and

their causal effects for a given forward pass. A common approach to construct computational graphs is to replace model components with dense activations with a sparsely-activating approximation. [6] introduces Transcoders to approximate MLP layers, while [1] further develops Cross-layer Transcoders to handle inter-layer features. [18] uses Cross-layer Transcoders to conduct circuit analyses for a wide range of behaviors, such as multi-step reasoning (for factual recall) or addition, and also investigate when a model’s CoT is (un)faithful. In our work, we identify key components needed for a potentially larger verification circuit without the need for separate sparse approximations.

6 Discussion

We studied the verification mechanism in a task-specific model. We repurposed mode collapse as a feature, not a bug: by leveraging the fact that preference tuning leads to mode collapse, we train a model with highly structured CoT, making it easy to parse its reasoning trace. With this setup, we studied how the model verifies its own outputs. We found GLU weights that activate based on the correctness of the model’s CoT tokens, and previous-token heads that can disable verification. We offer a simple extension to inter-layer communication channels that allow us to localize as few as three attention heads that can also disable verification.

Note that we do not claim to have uncovered a full verification circuit, but rather critical components and subspaces needed for verification. We also reiterate the scope of our work: we study a specific task that allows for **context-based verification**, while obviously not all reasoning tasks share this property. Namely, many tasks likely require **prior-based verification** using general knowledge. We speculate that similar components and subspaces are used for prior-based verification tasks as well, but is less obvious where those latents show up.

Lastly, though we only study a single model, we expect our findings to generalize to other models, given that the hidden states of language models often share the same geometry [16].

With that said, we view our work as a step towards understanding the inner mechanisms of recent reasoning models.

Acknowledgments

AL acknowledges support from the Superalignment Fast Grant from OpenAI. MW and FV acknowledge support from the Superalignment Fast Grant from OpenAI, Effective Ventures Foundation, Effektiv Spenden Schweiz, and the Open Philanthropy Project. All experiments were conducted on the FASRC cluster supported by the FAS Division of Science Research Computing Group at Harvard University and the University of Chicago AI Cluster.

References

- [1] Emmanuel Ameisen, Jack Lindsey, Adam Pearce, Wes Gurnee, Nicholas L. Turner, Brian Chen, Craig Citro, David Abrahams, Shan Carter, Basil Hosmer, Jonathan Marcus, Michael Sklar, Adly Templeton, Trenton Bricken, Callum McDougall, Hoagy Cunningham, Thomas Henighan, Adam Jermy, Andy Jones, Andrew Persic, Zhenyi Qi, T. Ben Thompson, Sam Zimmerman, Kelley Rivoire, Thomas Conerly, Chris Olah, and Joshua Batson. Circuit tracing: Revealing computational graphs in language models. *Transformer Circuits Thread*, 2025.
- [2] Iván Arcuschin, Jett Janiak, Robert Krzyzanowski, Senthoran Rajamanoharan, Neel Nanda, and Arthur Conmy. Chain-of-thought reasoning in the wild is not always faithful. *arXiv preprint arXiv:2503.08679*, 2025.
- [3] Andy Arditi, Oscar Balcells Obeso, Aaquib Syed, Daniel Paleka, Nina Rimsky, Wes Gurnee, and Neel Nanda. Refusal in language models is mediated by a single direction. In *The Thirty-eighth Annual Conference on Neural Information Processing Systems*.
- [4] Collin Burns, Haotian Ye, Dan Klein, and Jacob Steinhardt. Discovering latent knowledge in language models without supervision. In *The Eleventh International Conference on Learning Representations*.
- [5] Yida Chen, Aoyu Wu, Trevor DePodesta, Catherine Yeh, Kenneth Li, Nicholas Castillo Marin, Oam Patel, Jan Riecke, Shivam Raval, Olivia Seow, et al. Designing a dashboard for transparency and control of conversational ai. *arXiv preprint arXiv:2406.07882*, 2024.
- [6] Jacob Dunefsky, Philippe Chlenski, and Neel Nanda. Transcoders find interpretable llm feature circuits. In *The Thirty-eighth Annual Conference on Neural Information Processing Systems*.
- [7] Nelson Elhage, Neel Nanda, Catherine Olsson, Tom Henighan, Nicholas Joseph, Ben Mann, Amanda Askell, Yuntao Bai, Anna Chen, Tom Conerly, Nova DasSarma, Dawn Drain, Deep Ganguli, Zac Hatfield-Dodds, Danny Hernandez, Andy Jones, Jackson Kernion, Liane Lovitt, Kamal Ndousse, Dario Amodei, Tom Brown, Jack Clark, Jared Kaplan, Sam McCandlish, and Chris Olah. A mathematical framework for transformer circuits. *Transformer Circuits Thread*, 2021. <https://transformer-circuits.pub/2021/framework/index.html>.
- [8] Javier Ferrando, Oscar Obeso, Senthoran Rajamanoharan, and Neel Nanda. Do i know this entity? knowledge awareness and hallucinations in language models. *arXiv preprint arXiv:2411.14257*, 2024.
- [9] Kanishk Gandhi, Ayush Chakravarthy, Anikait Singh, Nathan Lile, and Noah D Goodman. Cognitive behaviors that enable self-improving reasoners, or, four habits of highly effective stars. *arXiv preprint arXiv:2503.01307*, 2025.
- [10] Kanishk Gandhi, Denise Lee, Gabriel Grand, Muxin Liu, Winson Cheng, Archit Sharma, and Noah D Goodman. Stream of search (sos): Learning to search in language. *arXiv preprint arXiv:2404.03683*, 2024.
- [11] Daya Guo, Dejian Yang, Haowei Zhang, Junxiao Song, Ruoyu Zhang, Runxin Xu, Qihao Zhu, Shirong Ma, Peiyi Wang, Xiao Bi, et al. Deepseek-r1: Incentivizing reasoning capability in llms via reinforcement learning. *arXiv preprint arXiv:2501.12948*, 2025.
- [12] Dan Hendrycks and Kevin Gimpel. Gaussian error linear units (gelus). *arXiv preprint arXiv:1606.08415*, 2016.
- [13] Robert Kirk, Ishita Mediratta, Christoforos Nalmpantis, Jelena Luketina, Eric Hambro, Edward Grefenstette, and Roberta Raileanu. Understanding the effects of rlhf on llm generalisation and diversity. In *The Twelfth International Conference on Learning Representations*, 2024.
- [14] Tamera Lanham, Anna Chen, Ansh Radhakrishnan, Benoit Steiner, Carson Denison, Danny Hernandez, Dustin Li, Esin Durmus, Evan Hubinger, Jackson Kernion, et al. Measuring faithfulness in chain-of-thought reasoning. *arXiv preprint arXiv:2307.13702*, 2023.

- [15] Andrew Lee, Xiaoyan Bai, Itamar Pres, Martin Wattenberg, Jonathan K Kummerfeld, and Rada Mihalcea. A mechanistic understanding of alignment algorithms: A case study on dpo and toxicity. In *International Conference on Machine Learning*, pages 26361–26378. PMLR, 2024.
- [16] Andrew Lee, Melanie Weber, Fernanda Viégas, and Martin Wattenberg. Shared global and local geometry of language model embeddings. *arXiv preprint arXiv:2503.21073*, 2025.
- [17] Kenneth Li, Oam Patel, Fernanda Viégas, Hanspeter Pfister, and Martin Wattenberg. Inference-time intervention: Eliciting truthful answers from a language model. *Advances in Neural Information Processing Systems*, 36:41451–41530, 2023.
- [18] Jack Lindsey, Wes Gurnee, Emmanuel Ameisen, Brian Chen, Adam Pearce, Nicholas L. Turner, Craig Citro, David Abrahams, Shan Carter, Basil Hosmer, Jonathan Marcus, Michael Sklar, Adly Templeton, Trenton Bricken, Callum McDougall, Hoagy Cunningham, Thomas Henighan, Adam Jermy, Andy Jones, Andrew Persic, Zhenyi Qi, T. Ben Thompson, Sam Zimmerman, Kelley Rivoire, Thomas Conerly, Chris Olah, and Joshua Batson. On the biology of a large language model. *Transformer Circuits Thread*, 2025.
- [19] Jack Merullo, Carsten Eickhoff, and Ellie Pavlick. Talking heads: Understanding inter-layer communication in transformer language models. *Advances in Neural Information Processing Systems*, 37:61372–61418, 2024.
- [20] Tomas Mikolov, Kai Chen, Greg Corrado, and Jeffrey Dean. Efficient estimation of word representations in vector space. *arXiv preprint arXiv:1301.3781*, 2013.
- [21] Sonia K Murthy, Tomer Ullman, and Jennifer Hu. One fish, two fish, but not the whole sea: Alignment reduces language models’ conceptual diversity. *arXiv preprint arXiv:2411.04427*, 2024.
- [22] Neel Nanda, Andrew Lee, and Martin Wattenberg. Emergent linear representations in world models of self-supervised sequence models. In *Proceedings of the 6th BlackboxNLP Workshop: Analyzing and Interpreting Neural Networks for NLP*, pages 16–30, 2023.
- [23] Nostalgebraist. Interpreting gpt: The logit lens, 2020.
- [24] Chris Olah, Nick Cammarata, Ludwig Schubert, Gabriel Goh, Michael Petrov, and Shan Carter. Zoom in: An introduction to circuits. *Distill*, 2020. <https://distill.pub/2020/circuits/zoom-in>.
- [25] Bruno A. Olshausen and David J. Field. Sparse coding with an overcomplete basis set: A strategy employed by v1? *Vision Research*, 37(23):3311–3325, 1997.
- [26] Catherine Olsson, Nelson Elhage, Neel Nanda, Nicholas Joseph, Nova DasSarma, Tom Henighan, Ben Mann, Amanda Askell, Yuntao Bai, Anna Chen, Tom Conerly, Dawn Drain, Deep Ganguli, Zac Hatfield-Dodds, Danny Hernandez, Scott Johnston, Andy Jones, Jackson Kernion, Liane Lovitt, Kamal Ndousse, Dario Amodei, Tom Brown, Jack Clark, Jared Kaplan, Sam McCandlish, and Chris Olah. In-context learning and induction heads. *Transformer Circuits Thread*, 2022. <https://transformer-circuits.pub/2022/in-context-learning-and-induction-heads/index.html>.
- [27] OpenAI. Learning to reason with llms. <https://openai.com/index/learning-to-reason-with-llms/>. Accessed: 2025-03-21.
- [28] Hadas Orgad, Michael Toker, Zorik Gekhman, Roi Reichart, Idan Szpektor, Hadas Kotek, and Yonatan Belinkov. Llms know more than they show: On the intrinsic representation of llm hallucinations. *arXiv preprint arXiv:2410.02707*, 2024.
- [29] Vishakh Padmakumar and He He. Does writing with language models reduce content diversity? In *The Twelfth International Conference on Learning Representations*, 2024.
- [30] Kiho Park, Yo Joong Choe, and Victor Veitch. The linear representation hypothesis and the geometry of large language models. In *Forty-first International Conference on Machine Learning*.

- [31] Tian Qin, David Alvarez-Melis, Samy Jelassi, and Eran Malach. To backtrack or not to backtrack: When sequential search limits model reasoning. *arXiv preprint arXiv:2504.07052*, 2025.
- [32] Nina Rimskey, Nick Gabrieli, Julian Schulz, Meg Tong, Evan Hubinger, and Alexander Turner. Steering llama 2 via contrastive activation addition. In *Proceedings of the 62nd Annual Meeting of the Association for Computational Linguistics (Volume 1: Long Papers)*, pages 15504–15522, 2024.
- [33] Noam Shazeer. Glu variants improve transformer. *arXiv preprint arXiv:2002.05202*, 2020.
- [34] Stewart Slocum, Asher Parker-Sartori, and Dylan Hadfield-Menell. Diverse preference learning for capabilities and alignment. In *The Thirteenth International Conference on Learning Representations*, 2025.
- [35] Curt Tigges, Oskar John Hollinsworth, Atticus Geiger, and Neel Nanda. Linear representations of sentiment in large language models. *CoRR*, 2023.
- [36] Miles Turpin, Julian Michael, Ethan Perez, and Samuel Bowman. Language models don’t always say what they think: Unfaithful explanations in chain-of-thought prompting. *Advances in Neural Information Processing Systems*, 36:74952–74965, 2023.
- [37] Constantin Venhoff, Iván Arcuschin, Philip Torr, Arthur Conmy, and Neel Nanda. Understanding reasoning in thinking language models via steering vectors. In *Workshop on Reasoning and Planning for Large Language Models*, 2025.
- [38] Jason Wei, Xuezhi Wang, Dale Schuurmans, Maarten Bosma, Fei Xia, Ed Chi, Quoc V Le, Denny Zhou, et al. Chain-of-thought prompting elicits reasoning in large language models. *Advances in neural information processing systems*, 35:24824–24837, 2022.
- [39] Shunyu Yao, Dian Yu, Jeffrey Zhao, Izhak Shafran, Tom Griffiths, Yuan Cao, and Karthik Narasimhan. Tree of thoughts: Deliberate problem solving with large language models. *Advances in neural information processing systems*, 36:11809–11822, 2023.
- [40] Anqi Zhang, Yulin Chen, Jane Pan, Chen Zhao, Aurojit Panda, Jinyang Li, and He He. Reasoning models know when they’re right: Probing hidden states for self-verification. *arXiv preprint arXiv:2504.05419*, 2025.
- [41] Andy Zou, Long Phan, Sarah Chen, James Campbell, Phillip Guo, Richard Ren, Alexander Pan, Xuwang Yin, Mantas Mazeika, Ann-Kathrin Dombrowski, et al. Representation engineering: A top-down approach to ai transparency. *arXiv preprint arXiv:2310.01405*, 2023.

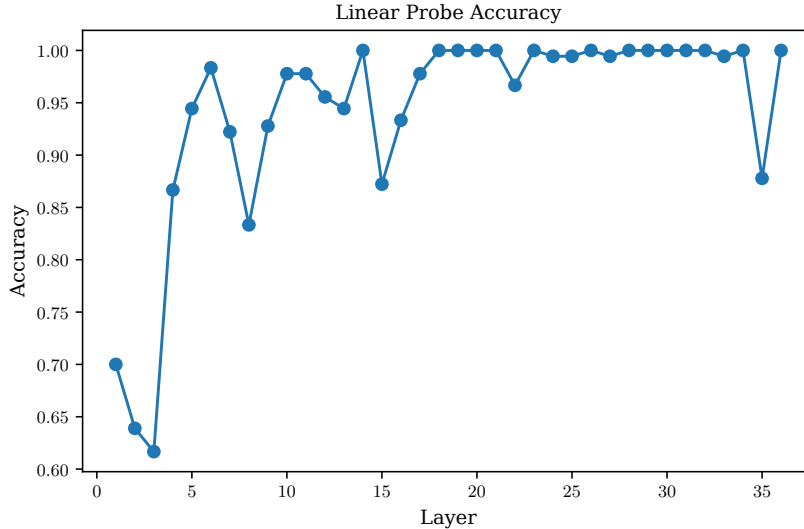


Figure 4: **Probe Accuracy.** The model has a linear separation in its hidden states given correct versus incorrect CoT tokens.

A Hyperparameters for Probing

We use a batch size of 8, validation size of 256, weight decay of 0.01, and learning rate of 1e-4. We validate every 50 gradient steps, and terminate training when validation loss has not improved after a patience value of 10.

B Probe Accuracy

Figure 4 shows probing results. The model has a linear separation in its hidden states given correct versus incorrect CoT tokens.

C Examples of Steering Verification with Probe

Once we identify a direction that encodes solved versus unsolved states (i.e., W_{probe}), we can simply add this direction into the model’s hidden states to make the model believe that it has found a solution:

$$\mathbf{x}^\ell = \mathbf{x}^\ell + \alpha W_{probe} \quad (11)$$

where $\mathbf{x}^\ell, W_{probe} \in \mathbb{R}^d$ and $\alpha \in \mathbb{R}$. Some hyperparameters include ℓ (which layers to steer on) and α , where a larger α amplifies the target behavioral effect.

While an extensive hyperparameter search and a systematic experiment may be useful, steering is not a core component but rather a tangential experiment. We thus provide qualitative examples using $\ell = \{n \mid 24 \leq n \leq 36\}$ and $\alpha = 20$ (after normalizing W_{probe}) in Table 3.

D Alternative Subsets of Previous-Token Heads

Of the 25 previous-token heads that we identify, there are many ways to identify subsets that disable verification. We offer a few examples, and document how many heads are needed to disable verification with perfect success rates (including partial successes).

Attention Density. The simplest method is to sort the heads based on how much they attend to the target token that timestep t_{ans} .

Varying Hyperparameters. Given our approach (Section 4.3), we try different parameters for N.

Sort by Similarity to W_{gate}, W_{up} . An alternative approach is to sort the attention heads based on how similar their OV circuits are to the W_{gate} and W_{up} weights of the GLU_{Valid} weights. We simply take the mean of $\{W_{gate}^i, W_{up}^i\}_i^N$ vectors from our N GLU_{Valid} weights. We then sort attention heads based on how similar they are to the resulting mean vector.

Sort by Probe W_{Probe} . An alternative is to sort the attention heads based on how similar their OV circuits are to the probe vector W_{Probe} .

Table 4 demonstrates how many heads are needed from each approach to disable verification with perfect accuracy.

Operands	Target	Type	Output
3, 87, 38	46	Orig.	$\langle \text{think} \rangle$ $87 - 38 - 3 = 116 - 3 = 113$ (not 46) $87 - 38 + 3 = 49 + 3 = 52$ (not 46) $87 - 38 + 3 = 49 + 3 = 52$ (not 46) $87 + 38 - 3 = 125 - 3 = 122$ (not 46) $38 + 38 - 3 = 76 - 3 = 73$ (not 46)...
		Steer	$\langle \text{think} \rangle$ $87 - 38 - 3 = 116 - 3 = 113$ (not 46) $87 - 38 + 3 = 49 + 3 = 52$ (not 46) $87 - 38 + 3 = 49 + 3 = 52!$ Yes, we got it! $87 - 38 + 3 = 49 + 3 = 52.$ $\langle \text{think} \rangle$ $\langle \text{answer} \rangle 87 - 38 + 3 \langle \text{answer} \rangle$
60, 62, 12, 34	68	Orig.	$\langle \text{think} \rangle$ $60 - 62 + 12 + 34 = 54 + 12 + 34 = 66 + 34 = 100$ (not 68) $60 + 62 - 12 - 34 = 122 - 12 - 34 = 108 - 34 = 74 - 34 = 40$ (not 68) $60 + 62 - 34 + 12 = 122 - 34 + 12 = 88 + 12 = 100 - 34 = 66$ (not 68) $60 + 34 + 12 - 62 = 94 + 12 - 62 = 106 - 62 = 44$ (not 68)...
		Steer	$\langle \text{think} \rangle$ $60 - 62 + 12 + 34 = 54 + 12 + 34 = 66 + 34 = 100$ (not 68) $60 + 62 - 12 - 34 = 122 - 12 - 34 = 108 - 34 = 74 - 34 = 40$ (not 68) $60 + 62 - 34 + 12 = 122 - 34 + 12 = 88 + 12 = 100 - 34 = 66$ exactly! So the equation that equals 68 is: $60 + 62 - 34 + 12$ $\langle \text{think} \rangle$ $\langle \text{answer} \rangle 60 + 62 - 32 + 12 \langle \text{answer} \rangle$
30, 90, 27, 19	74	Orig.	$\langle \text{think} \rangle$ $90 - 30 - 27 + 19 = 60 - 27 + 19 = 33 + 19 = 52$ (not 74) $90 - 30 - 27 + 19 = 60 - 27 + 19 = 33 + 19 = 52$ (not 74) $90 - 30 - 27 + 19 = 60 - 27 + 19 = 33 + 19 = 52$ (not 74) $90 + 27 + 19 - 30 = 117 + 19 - 30 = 136 - 30 = 106$ (not 74)...
		Steer	$\langle \text{think} \rangle$ $90 - 30 - 27 + 19 = 60 - 27 + 19 = 33 + 19 = 52$ (not 74) $90 - 30 - 27 + 19 = 60 - 27 + 19 = 33 + 19 = 52!$ Indeed, $90 - 30 - 27 + 19 = 60 - 27 + 19 = 33 + 19 = 52$ So, let's try another combination: $90 - 30 - 27 + 19 = 60 - 27 + 19 = 33 + 19 = 52$ No luck. Let's try this: $90 - 30 - 27 + 19 = 60 - 27$

Table 3: Steering with probe W_{probe} .

Method	Num. Heads	Heads
Eq. 9 (N=200)	3	L17H14, L17H11, L17H10
Eq. 9 (N=50)	15	L12H3, L12H8, L11H8, L17H1, L17H3, L10H5, L17H10, L17H11, L17H13, L21H10, L19H8, L13H3, L13H6, L5H15, L17H14
Eq. 9 (N=100)	100	L17H3, L17H1, L12H8, L17H10, L17H14, L17H11
Eq. 9 (N=300)	12	L17H14, L5H15, L19H13, L5H14, L13H6, L17H11, L15H8, L13H3, L19H8, L4H5, L17H3, L17H10
Attention Density	8	L17H14, L17H10, L13H3, L13H6, L5H14, L19H8, L4H3, L22H14
Sort by W_{gate}, W_{up}	17	L18H3, L21H7, L12H8, L21H14, L22H14, L11H8, L21H10, L12H3, L15H15, L17H3, L17H14, L15H8, L5H15, L13H6, L17H11, L19H13, L19H8
Sort by W_{Probe}	17	L18H7, L21H2, L22H12, L17H13, L17H11, L17H10, L4H5, L15H8, L17H14, L5H14, L22H14, L13H5, L5H15, L10H5, L15H15, L19H13, L13H6

Table 4: **Alternative approaches to localize attention heads that disable verification**, and the number of heads required to disable verification.